

# Correlation steering in the angularly multimode Raman atomic memory

MATEUSZ MAZELANIK, MICHAŁ DĄBROWSKI,\* AND WOJCIECH WASILEWSKI

*Institute of Experimental Physics, Faculty of Physics, University of Warsaw, Pasteura 5, 02-093 Warsaw, Poland*

\**mdabrowski@fuw.edu.pl*

**Abstract:** We present the possibility of steering the direction of correlations between the off-resonant Raman scattered photons from the angularly multimode atomic memory based on warm rubidium vapors. Using acousto-optic deflectors (AOD) driven by different modulation frequencies we experimentally change the angle of incidence of the laser beams on the atomic ensemble. Performing correlations measurements for various deflection angles we verify that we can choose the anti-Stokes light propagation direction independently of the correlated Stokes scattered light in the continuous way. As a result we can select the spatial mode of photons retrieved from the memory, which may be important for future development of quantum information processing.

© 2024 Optical Society of America

**OCIS codes:** (270.5585) Quantum information and processing; (020.0020) Quantum optics; (230.1040) Atomic and molecular physics; (290.5910) Scattering, stimulated Raman; (270.0270) Acousto-optical devices.

## References and links

1. C. H. Bennett, "Quantum cryptography using any two nonorthogonal states," *Phys. Rev. Lett.* **68**(21), 3121–3124 (1992).
2. N. Gisin, G. Ribordy, W. Tittel, and H. Zbinden, "Quantum cryptography," *Rev. Mod. Phys.* **74**(1), 145–195 (2002).
3. E. Knill, R. Laflamme, and G. J. Milburn, "A scheme for efficient quantum computation with linear optics," *Nature* **409**(6816), 46–52 (2001).
4. P. Kok, W. J. Munro, K. Nemoto, T. C. Ralph, J. P. Dowling, and G. J. Milburn, "Linear optical quantum computing with photonic qubits," *Rev. Mod. Phys.* **79**(1), 135–174 (2007).
5. L. M. Duan, M. D. Lukin, J. I. Cirac, and P. Zoller, "Long-distance quantum communication with atomic ensembles and linear optics," *Nature* **414**(6862), 413–8 (2001).
6. P. G. Kwiat, K. Mattle, H. Weinfurter, A. Zeilinger, A. V. Sergienko, and Y. Shih, "New High-Intensity Source of Polarization-Entangled Photon Pairs," *Phys. Rev. Lett.* **75**(24), 4337–4341 (1995).
7. A. B. U'Ren, C. Silberhorn, K. Banaszek, and I. A. Walmsley, "Efficient conditional preparation of high-fidelity single photon states for fiber-optic quantum networks," *Phys. Rev. Lett.* **93**(9), 093601 (2004).
8. A. B. U'Ren, Y. Jeronimo-Moreno, and H. Garcia-Gracia, "Generation of Fourier-transform-limited heralded single photons," *Phys. Rev. A* **75**(2), 023810 (2007).
9. M. A. Broome, M. P. Almeida, A. Fedrizzi, and A. G. White, "Reducing multi-photon rates in pulsed down-conversion by temporal multiplexing," *Opt. Express* **19**(23), 22698 (2011).
10. M. A. Hall, J. B. Altepeter, and P. Kumar, "Ultrafast switching of photonic entanglement," *Phys. Rev. Lett.* **106**(5), 053901 (2011).
11. X.-S. Ma, S. Zotter, J. Kofler, T. Jennewein, and A. Zeilinger, "Experimental generation of single photons via active multiplexing," *Phys. Rev. A* **83**(4), 043814 (2011).
12. X.-C. Yao, T.-X. Wang, P. Xu, H. Lu, G.-S. Pan, X.-H. Bao, C.-Z. Peng, C.-Y. Lu, Y.-A. Chen, and J.-W. Pan, "Observation of eight-photon entanglement," *Nat. Photonics* **6**(4), 225–228 (2012).
13. M. J. Collins, C. Xiong, I. H. Rey, T. D. Vo, J. He, S. Shahnian, C. Reardon, T. F. Krauss, M. J. Steel, A. S. Clark, and B. J. Eggleton, "Integrated spatial multiplexing of heralded single-photon sources," *Nat. Commun.* **4**, 2582 (2013).
14. J. Nunn, N. K. Langford, W. S. Kolthammer, T. F. M. Champion, M. R. Sprague, P. S. Michelberger, X.-M. Jin, D. G. England, and I. A. Walmsley, "Enhancing multiphoton rates with quantum memories," *Phys. Rev. Lett.* **110**(13), 133601 (2013).
15. S.-Y. Lan, A. G. Radnaev, O. A. Collins, D. N. Matsukevich, T. A. Kennedy, and A. Kuzmich, "A multiplexed quantum memory," *Opt. Express* **17**(16), 13639 (2009).
16. O. A. Collins, S. D. Jenkins, A. Kuzmich, and T. A. B. Kennedy, "Multiplexed memory-insensitive quantum repeaters," *Phys. Rev. Lett.* **98**(6), 060502 (2007).

17. K. Surmacz, J. Nunn, K. Reim, K. C. Lee, V. O. Lorenz, B. Sussman, I. A. Walmsley, and D. Jaksch, “Efficient spatially resolved multimode quantum memory,” *Phys. Rev. A* **78**(3), 033806 (2008).
  18. D. B. Higginbottom, B. M. Sparkes, M. Rancic, O. Pinel, M. Hosseini, P. K. Lam, and B. C. Buchler, “Spatial-mode storage in a gradient-echo memory,” *Phys. Rev. A* **86**(2), 023801 (2012).
  19. M. Shuker, O. Firstenberg, R. Pugatch, A. Ron, and N. Davidson, “Storing Images in Warm Atomic Vapor,” *P Phys. Rev. Lett.* **100**(22), 223601 (2008).
  20. M. T. Turnbull, P. G. Petrov, C. S. Embrey, A. M. Marino, and V. Boyer, “Role of the phase-matching condition in nondegenerate four-wave mixing in hot vapors for the generation of squeezed states of light,” *Phys. Rev. A* **88**(3), 033845 (2013).
  21. M. Parniak, A. Leszczyński, and W. Wasilewski, “Coupling of four-wave mixing and Raman scattering by ground-state atomic coherence,” *Phys. Rev. A* **93**(5), 053821 (2016).
  22. R. Chrapkiewicz and W. Wasilewski, “Generation and delayed retrieval of spatially multimode Raman scattering in warm rubidium vapors,” *Opt. Express* **20**(28), 29540 (2012).
  23. M. Dąbrowski, R. Chrapkiewicz, and W. Wasilewski, “Magnetically tuned, robust and efficient filtering system for spatially multimode quantum memory in warm atomic vapors,” *J. Mod. Opt.* (to be published).
  24. R. Chrapkiewicz, W. Wasilewski, and K. Banaszek, “High-fidelity spatially resolved multiphoton counting for quantum imaging applications,” *Opt. Lett.* **39**(17), 5090–3 (2014).
  25. M. Jachura and R. Chrapkiewicz, “Shot-by-shot imaging of Hong-Ou-Mandel interference with an intensified sCMOS camera,” *Opt. Lett.* **40**(7), 1540–3 (2015).
  26. M. Dąbrowski, R. Chrapkiewicz, and W. Wasilewski, “Hamiltonian design in readout from room-temperature Raman atomic memory,” *Opt. Express* **22**(21), 26076–90 (2014).
  27. K. O. Roberts, T. McKellar, J. Fekete, A. Rakonjac, A. B. Deb, and N. Kjærgaard, “Steerable optical tweezers for ultracold atom studies,” *Opt. Lett.* **39**(7), 2012–5 (2014).
  28. R. Chrapkiewicz, M. Dąbrowski, and W. Wasilewski, “High-Capacity Angularly-Multiplexed Holographic Memory for Enhanced-Rate Generation of Photons,” <http://www.arxiv.org/abs/1604.06049>.
  29. R. Chrapkiewicz, W. Wasilewski, and C. Radzewicz, “How to measure diffusional decoherence in multimode rubidium vapor memories?” *Opt. Commun.* **317**, 1–6 (2014).
- 

## 1. Introduction

### 1.1. State of the art and motivation

Single photon sources are essential elements of quantum information processing (QIP) architecture. They play inevitable role in quantum key distribution [1,2], quantum linear computing [3,4] and communication [5]. So far spontaneous parametric down-conversion (SPDC) sources remain most widespread [6–8].

The quantum state of a photon pair produced in SPDC is well defined and quite easy to engineer with pulsed pumping [6]. This enables building heralded photon sources with proper spatio-temporal properties. However, such sources produce photons at random and rarely [9], if contribution from multiphoton states is to be negligible. Many heralded sources can be used with a fast single-photon switch [10, 11] which routes the photon from the source that luckily worked to a single output, increasing chance of photon generation. In practice, setups with at most four SPDC sources have been demonstrated [12, 13].

Another option consists in using many SPDC sources and quantum memories to accumulate photons and release them on demand [14]. Once a photon is emitted in any of  $M$  memory mode, one can use an active optical switch [10, 11] controlled by the triggering signal from the Stokes scattering, to route the anti-Stokes photon to a desired single output. Such operation essentially relies on a memory storage time which has to exceed nanoseconds-long reconfiguration time of the optical switch [10, 11]. The experimental realization of that proposal uses an external switch with a dozen distinct atomic ensembles inside a cold quantum memory system [15]. This may be potentially useful to provide enhancement of the entanglement swapping rate between the nodes of a quantum network [16].

### 1.2. The photon source

Here we propose a scheme equivalent to  $M$  pair-sources with a built-in switch and verify its main aspects in a macroscopic light regime, with  $10^3$  photons in each spatial mode. The key element

of the scheme is an angularly-multimode atomic memory [17], based on Raman scattering in warm atomic vapors, in which many independent modes are stored using only one atomic ensemble [18, 19]. By redirecting the readout laser beam we change the emission angle of photons at the readout stage of the memory. This way we combine an equivalent multiple photon sources, memories and a switch in a single cell. Such solution enables redirecting the retrieved photon to a single output fiber. Note that we operate on macroscopic light, instead of manipulating fragile quantum entities (e.g. single atomic excitations), that are prone to losses and decoherence during such a manipulation.

The concept is illustrated in Fig. 1(a) where we present three sequential realizations of the generation of a single photon using Raman scattering in an ensemble of rubidium-87 atoms. In each single realization we use write-in laser with the same wavevector  $\mathbf{k}_w$  to induce Stokes scattering. The probability of generating Stokes photon in a single spatial mode is kept very low (typically  $p \ll 1/100$ ) but the number of modes  $M$  can be high, so the probability of generating a photon in any mode  $Mp$  is significant. In some repetitions Stokes photon with wavevector  $\mathbf{k}_S$  is emitted in random direction and at the same time collective atomic excitation with wavevector  $\mathbf{K} = \mathbf{k}_r - \mathbf{k}_S$  is created. The atomic excitation can be stored for as long as the memory lifetime. Finally, the readout laser converts the atomic excitation to an anti-Stokes photon.

The direction of the anti-Stokes photon is determined by the directions of the Stokes photon and driving laser beams due to the time-delayed phase-matching conditions [20, 21] depicted in Fig. 1(b). As a result the anti-Stokes photon has a wavevector:

$$\mathbf{k}_{aS} = \mathbf{K} + \mathbf{k}_r = \mathbf{k}_w - \mathbf{k}_S + \mathbf{k}_r, \quad (1)$$

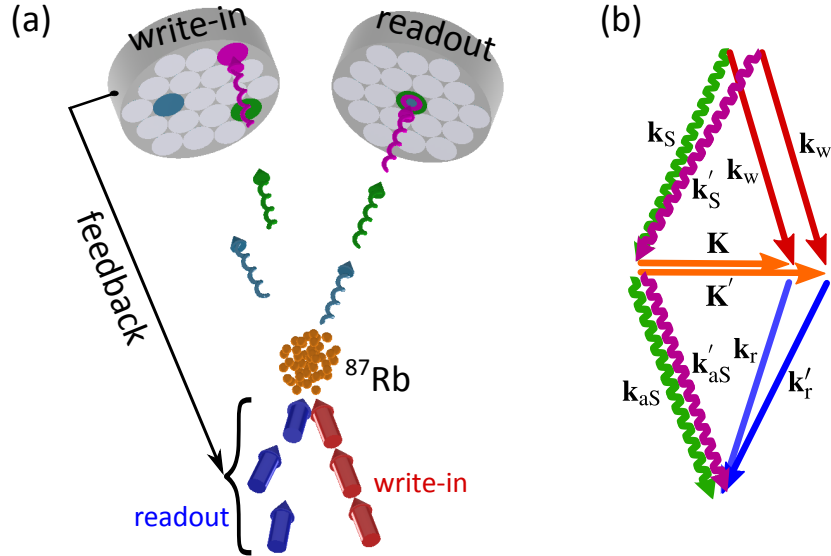


Fig. 1. Redirecting heralded photons into the same mode in warm rubidium vapors atomic memory. (a) Photons are scattered at random directions during the write-in process. By redirecting readout beam we can launch the readout photon into the same fiber each time. (b) Phase-matching in the Raman scattering process. The momenta difference between the write laser  $\mathbf{k}_w$  and scattered photon  $\mathbf{k}_S$  is stored in the spinwave wavevector  $\mathbf{K}$ . Then, it is added to the readout laser  $\mathbf{k}_r$ , leading to a well defined readout photon momentum  $\mathbf{k}_{aS}$ . For any write-in photon direction  $\mathbf{k}_S$  or  $\mathbf{k}'_S$  and any spinwaves with wavevectors  $\mathbf{K}$  or  $\mathbf{K}'$ , the direction of the readout beam can be adjusted accordingly from  $\mathbf{k}_r$  to  $\mathbf{k}'_r$  so as to preserve  $\mathbf{k}_{aS} = \mathbf{k}'_{aS}$ .

where  $\mathbf{k}_r$  is wavevector of the readout beam. Hence, even though the direction of the Stokes photon is random, the direction of the anti-Stokes photon can be controlled by sending the readout beam at a proper angle. As soon as we register a Stokes photon, we can calculate the wavevector difference  $\mathbf{K}$  stored inside the atoms. Next we compute the proper  $\mathbf{k}_r$  from Eq. 1 and shine the readout laser at an angle corresponding to this  $\mathbf{k}_r$ . This way the readout photon can be launched into the same fiber each time as depicted in Fig. 1(a).

## 2. Experiment

### 2.1. Off-resonant Raman scattering in $\Lambda$ -system

Our atomic memory scheme is based on off-resonant Raman scattering in  $\Lambda$ -system of rubidium-87 presented in the Fig. 2(a). Atoms are initially prepared in  $F = 1$  ground state sublevel by the optical pumping. The pumping laser is resonant with  $5^2S_{1/2}, F = 2 \rightarrow 5^2P_{3/2}$  transition of the D2-line (780 nm). The write-in laser at 795 nm is detuned from the  $F = 1 \rightarrow F' = 1$  transition of the D1-line to the red by  $\Delta_w = 1$  GHz and induces Stokes scattering. In this process the Stokes photons are created together with spinwaves corresponding to a coherent excitation of atoms into  $F = 2$  ground-state sublevel. We stop the write-in process after a few microseconds during which macroscopic amount of light is scattered. After an adjustable amount of time we illuminate the atomic ensemble with the readout laser, which drives the anti-Stokes scattering. This readout laser at 780 nm is detuned from the  $5^2S_{1/2}, F = 2 \rightarrow 5^2P_{3/2}$  to the blue by  $\Delta_r = 1$  GHz and creates an anti-Stokes photon at the expense of annihilating the atomic spinwave.

### 2.2. Experimental setup details

The experimental setup is depicted in Fig. 2(b). We use 16 mW write-in and readout laser power each and 70 mW power of pumping laser. The  $2w_0$  beams diameters inside memory cell were 7 mm, 7 mm and 12 mm, respectively. All of the lasers are frequency stabilized using DAVLL (Dichroic Atomic Vapor Laser Lock) scheme or saturation spectroscopy. The laser beams are initially filtered using Fabry-Pérot interferometers and then they pass through the AODs. We use an atomic memory cell with a length of  $L = 10$  cm (which corresponds to Fresnel number  $\mathcal{F} \approx 150$ ), containing warm  $^{87}\text{Rb}$  vapors with 1 Torr pressure krypton as a buffer gas [22], heated to about 80 °C. The output light of the atomic memory cell is filtered out using a Wollaston prism, atomic absorption filter and a Faraday filter [23]. The temperature of atomic absorption filter

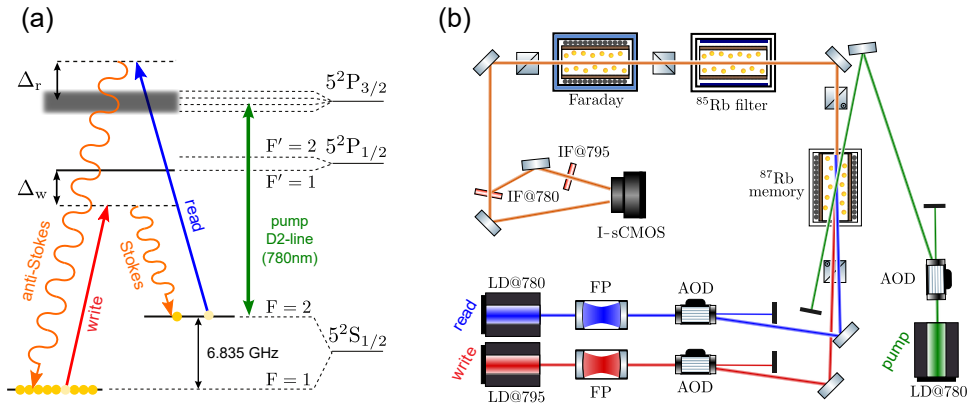


Fig. 2. (a) Atomic levels structure of rubidium-87 used in the experiment. (b) Experimental setup: LD – laser diodes, FP – Fabry-Pérot interferometer, AOD – acousto-optic deflector,  $^{87}\text{Rb}$  memory – atomic memory cell,  $^{87}\text{Rb}$  filter – absorption filter, Faraday – Faraday filter, IF – interference filter, I-sCMOS – sCMOS camera with image intensifier.

is set to 100 °C. Faraday filter also has a temperature of  $T = 100$  °C and magnetic field set to  $B = 12$  mT. Both the atomic memory cell and the Faraday filter were inside two layer magnetic shielding. The detunings ( $\Delta_w, \Delta_r$ ), the Faraday filter temperature and magnetic field was set to obtain the best signal to noise ratio. The Stokes was separated from the anti-Stokes light using 795 nm and 780 nm interference filters and both were directed into two separate regions on the camera. The camera pane could be divided into separate circular areas corresponding to distinct virtual fibers, presented in Fig. 4. The pulse sequence consisted of  $\tau_p = 350$   $\mu$ s pump pulse and  $\tau_w = \tau_r = 8$   $\mu$ s write-in and readout pulses, all of a rectangular shape. Memory storage time, i.e. delay between write-in and readout was equal to  $\tau_s = 1$   $\mu$ s. During the pulse sequence the cell heating was turned off to avoid the magnetic fields coming from the heating coils. Finally, the scattered photons were detected with an sCMOS (scientific Complementary Metal-Oxide Semiconductor) camera equipped with an image intensifier (I-sCMOS) [24, 25]. The gate of the image intensifier was open for the combined duration of the write-in, storage and readout pulses [26]. The image intensifier operated in the linear response regime.

### 2.3. Acousto-optic deflector (AOD)

Acousto-optic deflectors (AOD) were used to steer the laser beams directions [27] and produce microsecond driving pulses. The deflection angle is transferred into the center of the memory cell by a 4f relay lens system presented in Fig. 3. This particular deflection angle is changing by reconfiguring the electronic direct digital synthesizer (DDS), driving the deflector at a desired frequency. At last, the  $f_3$  lens focuses scattered photons, converting scattering angle into a position on the I-sCMOS sensor.

One can notice that in present solution beams deflected at different angles have different frequency. This frequency difference applies to anti-Stokes photons retrieved from the memory. However, this effect can be compensated by using additional AOD set in double pass system.

## 3. Results

### 3.1. Correlation measurements using camera

To verify the direction control ability of our photon source we calculated the correlations between the directions of scattered photons. In each iteration of the experiment we register an image formed by thousands of scattered photons which corresponds to an intensity of light  $I(\theta)$  emitted at a certain direction  $\theta = (\theta_x, \theta_y)$ . In the following we plot maps of correlation coefficient  $C(\theta, \theta')$  between light emitted at a fixed angle  $\theta'$  and light emitted at any other angle  $\theta$  [22, 26]:

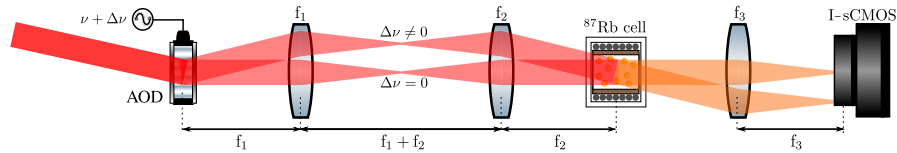


Fig. 3. The optical 4f relay transfers the angle of deflection of AOD into the centre of atomic memory. The deflection angle is proportional to AOD electrical drive frequency. The centre of AOD is optically imaged onto the center of atomic memory cell and next the crossing beams are projected onto I-sCMOS camera pane situated in the far-field with respect to the memory cell. The focal length of lenses:  $f_1 = 50$  mm,  $f_2 = 750$  mm,  $f_3 = 500$  mm. Basic modulation frequency was set to  $\nu = 80$  MHz, the laser beam diameter at the AOD input  $w = 250$   $\mu$ m. Such a configuration does not change the position of beams intersection inside memory cell but only changes the angle of crossing thus effectively changing the beams position in the far field camera.

$$C(\theta, \theta') = \frac{\langle I(\theta)I(\theta') \rangle - \langle I(\theta) \rangle \langle I(\theta') \rangle}{\sqrt{\langle (\Delta I(\theta))^2 \rangle \langle (\Delta I(\theta'))^2 \rangle}}, \quad (2)$$

where:  $I(\theta)$  is the mean intensity of light registered at angle  $\theta$  and  $\Delta I(\theta)$  is deviation from this mean value. The angles  $\theta$  are related to x and y components of wavevectors in Eq. (1) via a simple relation valid for small angles  $2\pi\theta = \mathbf{k}_\perp \lambda$ , where  $\lambda$  is the wavelength of the driving laser beam.

In the low gain regime one would measure the number of coincidences  $n(\theta, \theta')$  between the Stokes photon emitted at the angle  $\theta'$  and the anti-Stokes photon at the angle  $\theta$  [28]. In high gain regime pairing up photons is no longer possible, and a number of photons emitted in any direction appears to be random. However, the number of photons (i.e. intensity of light) emitted at angle  $\theta$  in each realization of the experiment should be in the ideal case equal to the number of photons emitted in the conjugate direction  $\theta' = -\theta$ .

### 3.2. Correlation maps

We measured the scattering angles for the direction of the write-in laser which was fixed during the experiment and central direction of the readout laser. When deflected, the readout laser was sent at angle  $\theta_{\text{read}} = (0, \Delta\theta_{\text{read}})$ , where  $\Delta\theta_{\text{read}}$  was controlled by the AOD system. In Fig. 4 we present maps of intensity correlation coefficient  $C(\theta, \theta')$  calculated from  $10^4$  camera frames.

Upper and lower parts of each panel depict correlations with light scattered during write-in and readout, respectively. Directions of the write-in and readout laser beams are marked as black crosses. The reference point  $\theta' = \Delta\theta_S$  is chosen in the write-in part of the camera pane. It can be identified with the position of the virtual fiber depicted as dashed circle that collects the heralding photons. The first row in the Fig. 4(a) presents correlation maps for stationary drive beams. In each panel we take different reference point  $\theta' = \Delta\theta_S$ .

Registration of a photon at a reference point corresponds to projecting the state of the atoms onto a spinwave. The spinwave is clipped to the size of the write-in beam of diameter  $2w_0$  and therefore its wavevector  $\mathbf{K}$  is defined with a finite precision  $\pm\lambda/w_0$ . This spinwave stimulates scattering of subsequent photons into a finite solid angle, corresponding to a certain angular spread of photons. The stimulated photons give rise to a finite-sized spot of Stokes-Stokes correlations around the reference direction  $\Delta\theta_S$  in upper parts of each panel. Note that they move around the reference direction. The twin spot located in the lower part of each panel attests the presence of correlated anti-Stokes photons. It moves in opposite direction  $\Delta\theta_{\text{as}} \approx -\Delta\theta_S$ , according to the phase-matching condition described by Eq. (1). Due to finite spatial size of the spinwave the anti-Stokes photons are emitted into a finite solid angle. Their angular spread is virtually the same as for the Stokes photons because they come from the same spinwave.

With Fig. 4(a) we verify that by registering a Stokes photon the direction of the anti-Stokes photon can be predicted. We can also see finite angular spread of the correlated photons which is a signature of a mode size and should match fiber mode to obtain best heralding efficiency. The number of modes  $M$  can be approximated as twice the number of correlation spots that fit into the solid angle occupied by the scattered light [22]. In the experiment we obtain  $M = 20$  and  $M = 10$  for write-in and readout processes, respectively. Virtual fibers depicted in Fig. 4 are placed with empty spaces between each other, thus the number of fibers is effectively lower than the number of modes.

In the second row of Fig. 4(b) we demonstrate manipulation of the emission angle of anti-Stokes light by changing the direction of readout laser  $\Delta\theta_{\text{read}}$ . We keep the reference point  $\theta' = \Delta\theta_S$  constant and thus the Stokes-Stokes correlations remain in place. The differences between this parameter in between panels are just the result of the uncertainty fitting Gaussian to the real data. However, the twin spot moves together with the read beam with constant scattering angle  $\Delta\theta_{\text{as}}$ , just as predicted by Eq. (1).

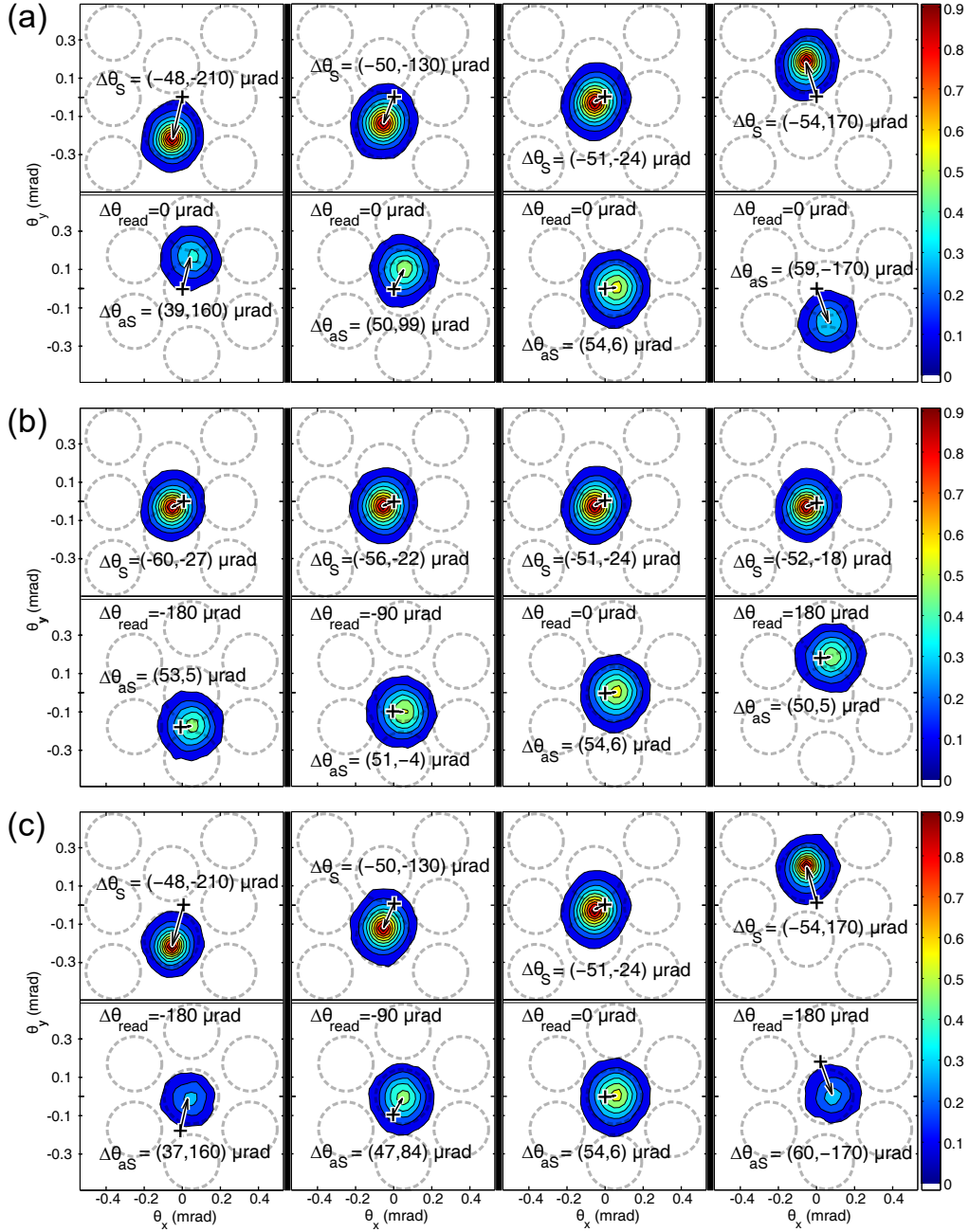


Fig. 4. Maps of correlations between intensity registered at a reference angle and the registered far field images around Stokes (write-in) driving beams (upper parts) and anti-Stokes (readout, lower parts). Rows represent situations with: (a) different reference angles  $\Delta\theta_S$ , (b) different AOD deflection angles  $\Delta\theta_{\text{read}}$ , (c) combination of reference points from (a) and deflection angles from (b) simultaneously, leading to static position of the twin spot center. That corresponds to coupling the light always into the same fiber of conceptual fiber matrix, depicted as dashed circles.

Finally, we verify the key aspect of the concept depicted in Fig. 1 using macroscopic Raman scattered light, with  $10^3$  photons generated per each spatial mode. In each panel of Fig. 4(c) we change reference point corresponding to a detection of a photon at different angle  $\Delta\theta_s$ . By redirecting the read beam we are able to redirect the twin photons into the same direction chosen arbitrary as  $(54, 6) \mu\text{rad}$ .

### 3.3. Cross-sections of correlation maps

Figure 5 depicts  $\theta_y$  cross-sections through twin beam correlation spot from Fig. 4 with fitted Gaussian curves. The angular spread of the correlation spot is about  $240 \mu\text{rad}$  FWHM. This correspond to an emission from an area of about  $3.5 \text{ mm}$  diameter. It is smaller by a factor of 2 than the write-in beam size due to exponential character of the Stokes scattering gain process. The spinwave is amplified primarily in the center of the laser beam and effectively shrinks. With our AOD system we can deflect anti-Stokes emission by about  $400 \mu\text{rad}$  with precision much better than the angular spread of the correlation. Figure 5(c) confirms that the anti-Stokes emission can be redirected into the same angular mode regardless of the position of the trigger photon. In Fig. 5(b) the maximum correlation value drops slightly for larger deflection angles  $|\Delta\theta_{\text{read}}|$ . This is the result of aberrations of our optical system. In Fig. 5(a) the maximum value of correlation coefficient drops at higher angles of scattering  $\Delta\theta_s$  because of diffusional damping of spinwaves with long wavevectors [22, 29].

### 3.4. Implications

The experimental results validate the scheme proposed in Fig. 1. The results presented in Figs. 4 and 5 enable designing the collection optics matching the photons to the single mode fibers. The focal length of the  $f_3$  lens should be chosen such that the size of the correlation spot matches the size of the fiber mode. Registering the trigger photon in any of the fibers heralds creation of a spinwave that covers always the same volume of the cell, but has different wavefront directions,

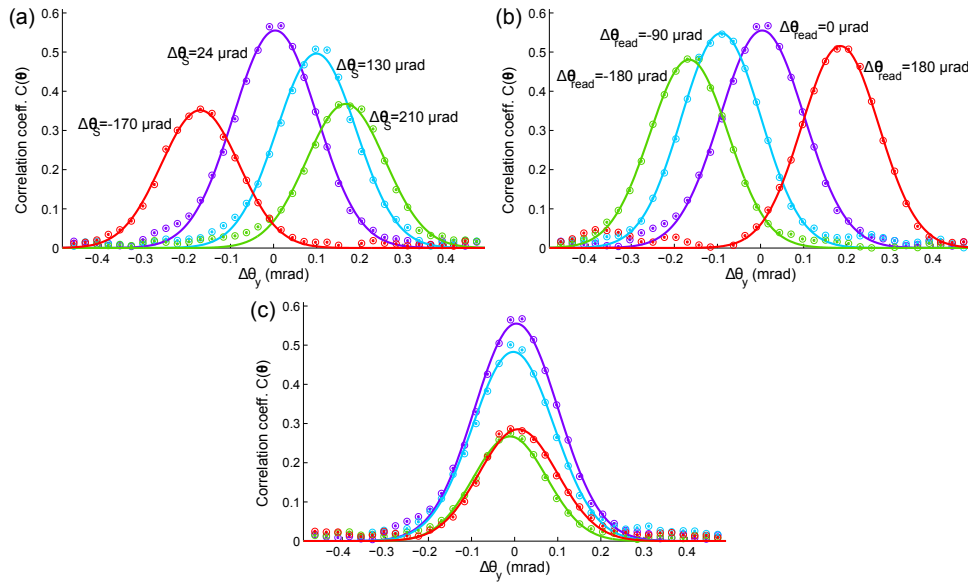


Fig. 5. Cross-sections of correlation maps from Fig. 4(a)-(c). The FWHM of correlation peak is about  $0.24 \text{ mrad}$ .



dependent of which fiber was hit. Its spatial phase corresponds to a plane-wave with wavevector  $\mathbf{K}$ . By adjusting the direction of the readout beam we can compensate spatial phase differences. That is between subsequent operations the wavevector of the readout beam  $\mathbf{k}_r$  is changed by precisely the same amount by which the spinwave wavevector  $\mathbf{K}$  is changed (compare Eq. (1)). This way at the readout stage the anti-Stokes field is emitted from the same volume and with the same spatial phase, always in the same spatial mode. Figures 4(c) and 5(c) effectively depict directional intensity profile of this mode. A proper optical setup can focus the anti-Stokes light into a spot matching always the same single mode fiber. By adjusting the write-in duration or power, the mean number of excitations  $\zeta$  created in each twin beams can be adjusted. By lowering this number to  $\zeta \lesssim 1/100$  we ensure, that in less than this amount of cases two photons would be generated instead of one, thus conditionally creating well defined single photon mode which state might be easily destroyed during the manipulation.

#### 4. Conclusions

We proposed a scheme for a single photon source equivalent to  $M$  heralded SPDC sources [14] and a switch realized in a single multimode emissive quantum memory. Similarly as in SPDC sources, the pair production rate per mode can be kept low enough to avoid double pair production. At the same time the total probability for photon generation in any mode can be high. In practice, demonstration of the whole scheme at the single photon level with real-time feedback requires better long term setup stability and faster detection time response of the sCMOS camera.

We populate random mode of the memory by driving Raman Stokes scattering. Upon registering the direction of scattered photon the mode which was excited is identified. Then the readout beam direction is adjusted and this way the readout is always launched in the same direction. The last step is an effective demultiplexing switch realized without directly operating on the fragile single photons.

The experimental verification demonstrated bases on measuring spatial intensity correlations. Our  $1 \mu\text{s}$  storage time is sufficient to switch the direction of the readout beam [15] and realize the scheme. In our demonstration we can retrieve about  $M = 10$  modes corresponding to independent pair sources. In the experiment, the number of excited modes is limited by the diffusion [29]. Therefore we expect the number of retrieved modes  $M$  to be lower than the Fresnel number  $\mathcal{F}$  of the write beam. We envisage that further increasing the drive beam sizes can lead to  $M = 1000$  modes, which would result in virtually deterministic single photon generation [28].

#### Funding

Polish National Science Centre projects no. DEC-2011/03/D/ST2/01941 and DEC-2015/19/N/ST2/01671.

#### Acknowledgments

We acknowledge A. Leszczyński, M. Lipka and M. Parniak for discussions about the manuscript.